

Supporting Information

Conversion of polyethylene terephthalate into pure terephthalic acid through synergy between a solid-degrading cutinase and a reaction intermediate-hydrolysing carboxylesterase

Arpita Mrigwani, Bhisem Thakur and Purnananda Guptasarma*

Centre for Protein Science, Design and Engineering (CPSDE),
Department of Biological Sciences,
Indian Institute of Science Education and Research (IISER) Mohali
Sector-81, SAS Nagar, Punjab 140306, India

Running Title: *A dissolved carboxylesterase aiding a plastic-bound cutinase*

* Corresponding Author

Email: guptasarma@iisermohali.ac.in; Phone: +91-172-2293151;

Webpage: www.guptasarmalab.in

Contents

Section 1. Green chemistry-related aspects of this work (Pages 3-8)

Section 2. Materials and methods (Pages 9-12)

Section 3. Tables (Page 13)

Table S1: Docking and binding scores.

Table S2: Thermal, kinetic and thermodynamic stabilities of TTCE and LCC.

Section 4. Figures (Pages 14-30)

Figure S1: Enzymatic breakdown of polyethylene terephthalate (PET)

Figure S2: RMSD and RMSF from molecular dynamics simulation of TTCE-2HE-(MHET)₄.

Figure S3: SDS-PAGE binding assay for LCC treated PET film (for a period of 8 hours).

Figure S4: Biophysical characterization of TTCE.

Figure S5: Thermal and thermodynamic stabilities of TTCE.

Figure S6: Chemical (equilibrium) stabilities of TTCE.

Figure S7: Chemical (kinetic) stability of TTCE.

Figure S8: Activity of TTCE upon different substrates.

Figure S9: Degradation of intact PET granules and post-consumer PET by TTCE and LCC.

Figure S10: Comparison of the activities of TTCE and LCC upon (A) para-nitrophenyl palmitate. (B) Fluorescein dilaurate. (C) Fluorescein di benzoate.

Figure S11: Synergistic action of LCC and TTCE (1 μ M each).

Figure S12: The PET-film bound fraction of the LCC-TTCE fusion construct.

Figure S13: Scanning electron microscopy images of enzyme treated PET films.

Figure S14: LC-coupled ESI Q-TOF MS based characterization of degradation products.

Figure S15: (A) LCC, (B) TTCE protein yields.

Section 5. References (Pages 30-32)

Section 1. Green chemistry related aspects of this work

Processing of post-consumer PET for degradation:

A summary of approaches used

- 1) **Mechanical treatment.** PET is turned into micron-sized beads through a process of crushing, rolling and milling.¹
- 2) **Heat treatment.** PET is decomposed either through pyrolysis (~400-600 °C), or through microwave treatment (160-250 °C) into terephthalic acid (TPA) and ethylene glycol (EG).²
- 3) **Thermo-chemical treatment.** A combination of chemicals and high temperatures is used to decompose PET. For example, (i) methanol treatment at 250-290 °C turns PET into dimethyl terephthalate (DMT) and ethylene glycol (EG), or (ii) treatment at 190 °C in ionic liquids such as supercritical ethanol with liquid 1-butyl, 3-methyl imidazolium tetrafluoroborate, or in the presence of the catalyst, zinc acetate, turns PET into bis-hydroxyethyl terephthalate (BHET).²

The above methods have recently been reviewed.²

[Damayanti and Ho-Shing Wu, *Polymers*, (2021) **13**, 1475-1512].

- 4) **Microbial/enzymatic treatment.** Microbe-secreted esterases act upon PET and the degradation intermediate, mono-hydroxyethyl terephthalate (MHET) is taken up by some fungi, actinomycetes, or preteobacteria (e.g., the organism, *Ideonella sakaiensis*). Inside the cell, other esterases turn MHET into protocatechuate (PCA) which enters the TCA cycle. This enables some microbes to degrade PET and use some degradation products as a source of carbon.³
- 5) **Pure enzymatic treatment.** Various esterase enzymes are currently being studied: (i) a cutinase, TfCut2, from *Thermobifida fusca*;³ (ii) a cutinase, LCC,³ derived from a metagenomic library created from leaf branch compost; (iii) a fusion enzyme consisting of a PET hydrolyzing esterase and a MHET-hydrolyzing esterase.⁴ Some fungus-derived enzymes are also being explored.⁵ Such enzymes bind to, and invade, solid crystalline PET at moderately high temperatures, to degrade it into a mixture of oligoethylene terephthalate (OET), BHET, MHET, TPA and EG.⁵

The above methods have recently been reviewed.³

[D. Danso, J. Chow, W.R. Streit, *Plastics: environmental and biotechnological perspectives on microbial degradation. Applied and Environmental Microbiology*, 2019, **85**:e01095-19].

PET enzymatic degradation/recycling:

A summary of (green chemistry-related) advantages

- 1) **Reduction in energy expenditure.** Use of lower temperatures. Cutinases/esterases from mesophile organisms (growth optima in the range of 20-60 °C) work optimally at temperatures in the range of 30-45 °C, and cutinase/esterases from thermophile organisms (growth optima in the range of 60-80 °C) work optimally at temperatures in the range of 50-70 °C.⁶ Thus, enzymes obviate the need to use high temperatures (> 400 °C for thermal decomposition of PET, and > 200 °C for thermo-chemical decomposition). It is sufficient to achieve temperatures approaching ~ 60-80 °C, to cause PET to undergo a glass-transition and expose the polymer backbone to enzymes. No need for stirring. Enzymes also obviate the need to use energy to stir reaction mixtures.⁷
- 2) **Reduction in cost of materials used.** Exploitation of microbes as low-cost enzyme-producing factories. Thermostable PET-degrading enzymes are produced as recombinant enzymes, through biosynthesis, i.e., through heterologous expression in mesophile organisms that grow upon low-cost nutritional substrates, at low temperatures,⁸ with each cell producing the desired enzyme at a

small fraction of the cost of producing the enzymes through chemical synthesis from amino acids.⁹ With an enzyme such as LCC, using 3 milligrams of which, i.e., 0.3 % (w/w) 1 gram of PET can be almost fully degraded,¹⁰ it is easy to produce 80-100 milligrams per litre of fermented *E. coli* culture, since 6-8 milligrams can be produced per litre of shake-flask cultures that allow one-fifteenth to one-twentieth of the growth achievable through high-density fermentation). With other enzymes, e.g., the TTCE enzyme used for the synergy demonstrated in this paper, the yields can be as much as four times this amount, in milligrams. *Exploitation of enzyme thermostability for low-cost purification.* The purification of recombinant thermostable enzymes produced by mesophile genetically-engineered microbial cell factories is of low cost due to the fact that cells can be heated to 60-70 °C to directly obtain enzyme of high purity, through thermal rupture of cells and denaturation and aggregation/precipitation of all cellular protein/enzyme constituents other than the desired (thermostable) enzyme, thus obviating the need for purification of enzymes by expensive chromatographic methods.¹¹

- 3) **Elimination of toxic/expensive chemicals and solvents.** Unlike chemical methods, enzymatic methods use aqueous environments, and require neither the presence of any expensive/toxic chemicals, nor the use of any expensive/toxic solvents.
- 4) **Enhanced scope for recycling.** Degradation of post-consumer PET by thermal and thermochemical means mostly results in the production of heterogeneous mixtures of TPA and other degradation intermediates (including side-products that are colored), although some expensive methods that are not commercially-viable do result in very high yields of TPA approaching 80-90 %.¹² The presence of side-products along with PET degradation intermediates in the TPA obtained through processing of post-consumer PET thus adversely affects the cost of production, and also the quality, of the PET that can be produced through recycling of such 'reclaimed' TPA.¹² In contrast, with enzymatic degradation, there are no side-products. If the yield of TPA from enzymatic degradation of PET can be improved to nearly one hundred percent, the PET that would be generated from such TPA is expected to be of comparable quality to virgin PET.¹⁰
- 5) **Reduced consumption of fossil fuel (petroleum).** PET is currently made from petroleum.¹³ Enzymatic degradation of PET into TPA which can be recycled into food-grade (virgin-like) PET is likely to reduce dependence on fossil fuel (petroleum) for the production of PET of acceptable quality through recycling, thus creating a viable circular economy involving PET and TPA that would reduce consumption of petroleum. Notably, it has been shown that the cost of production of new PET plastic from TPA generated through enzymatic degradation of post-consumer PET is about 4 % of the cost of production of fresh PET from petroleum.¹⁰
- 6) **Enhanced scope for valorization.** The TPA generated from PET through enzymatic degradation is of high-enough quality for it to also be turned into high-value aromatic products, or aromatic-derived products, such as protocatechuic acid (PCA), gallic acid (GA), pyrogallol, catechol, muconic acid (MA), and vanillic acid (VA).^{14,15} These are used in the manufacture of pharmaceuticals, cosmetics, sanitizers, animal feeds, bioplastic monomers, and so on.¹⁴

PET enzymatic degradation/recycling:

A summary of issues and previous attempts at resolution

Issues

- 1) **The generation of non-TPA intermediates, and the cost of separating TPA from these intermediates.** The main thing that appears to be currently holding back the recycling of PET in order to create a circular economy (with reduced dependence on fossil fuels, and increased prospects for valorization of TPA) is that enzymatic degradation of PET can occur upon a variety of different ester bonds in PET, and this causes the early stages of enzymatic degradation to inevitably produce not just pure TPA (which is the end product that is expected to result from the

breakage of all ester bonds in the PET backbone), but rather a mixture of oligoethylene terephthalate (OET), BHET, MHET, TPA and EG instead. Without separating TPA away from these other (intermediate) products of PET degradation, recycling of TPA into PET remains unviable, because separation is a costly proposition.^{16,17} What is needed is an enzymatic degradation system that leaves no intermediates. For this, it is necessary to pay attention to multiple possible ways in which such intermediates fail to be hydrolyzed to a significant degree.

- 2) **The inhibitory effect of non-TPA intermediates.** Certain degradation intermediates such as MHET appear to inhibit the PET-hydrolyzing activity of enzymes. In particular, TfCut2 displays significant MHET-based inhibition.¹⁸ Notably, LCC also shows MHET-based inhibition, although this is to a far lower degree than seen with TfCut2. Due to this, it is necessary to pay attention to multiple possible ways in which to either neutralize, overcome, or go around the problem of MHET-based inhibition.¹⁹

Attempts at resolving issues, and their outcomes

- 1) **Improvement of the PET-hydrolyzing activities of cutinase/esterase enzymes.** *Improvement of catalytic rates.* One approach that has been taken is to improve the enzymes that degrade PET, perhaps hoping that this would lead to more comprehensive degradation of both PET and its degradation intermediates. There is no doubt that this approach, involving both (a) the search for better enzymes, and (b) the improving of the activities and stabilities of such enzymes, through rational or combinatorial protein engineering, or other approaches, such as enzyme immobilization, has resulted in improvements in PET degradation. The search for better enzymes has led to the identification of TfCut2 from *Thermobifida fusca*, and LCC from a leaf branch compost metagenomic library.⁶ These are currently the leading naturally-occurring enzymes that have been identified, with LCC being clearly being more efficacious than TfCut2.¹⁰ Attempts have been made to improve both enzymes through protein engineering, and the current leading enzymes are variants of TfCut2 and LCC.^{10,19-22} Thus far, these improvements have managed to create a variant of LCC that is ~27 % more active (i.e., 1.27-fold more active) than LCC.¹⁰ *Improvement of enzyme stability - leading to longer timescales of activity, and to improved catalytic output.* Attempts have been made to improve the thermal stabilities of enzymes, with a view to increasing their longevity in reactions (and, therefore, their overall activity, as a function of the durations of reactions).¹⁰ *Improvement of PET binding leading to greater residence-times of enzymes upon solid PET, and to improved catalytic output.*^{23,24} Attempts have also been made to improve the PET-binding affinities of enzymes, with a view to increasing the residence time of enzymes upon PET, in order to improve the overall activity.

Outcome: Despite improvements in yields of TPA resulting from improvements in enzyme kinetic rates, enzyme thermal stabilities, and enzyme binding to PET, the generation of mixtures of degradation intermediates along with TPA remains a persistent issue. It has thus far not proved to be possible to generate pure TPA through enzymatic reactions. Basically, although it has been proved to be possible to improve the yields of TPA, this improvement has resulted in the concomitant improvement of the yields of the other intermediate degradation products as well.^{18,25} Thus, enzyme improvements have increased the production of TPA, but not improved the quality/purity of the generated TPA.

- 2) **Use of enzyme synergy, to reduce MHET inhibition.** It has been perceived that it could be useful to deploy a dual-enzyme system, i.e., to have an additional enzyme present along with cutinase engaged in PET hydrolysis (e.g., TfCut2, or LCC), to use this additional enzyme to reduce the amount of MHET, since MHET inhibits TfCut2 to a significant degree, and also inhibits LCC

(although to a lesser degree).¹⁸ Thus, an immobilized carboxylesterase has been used along with cutinase/esterase (either TfCut2, or LCC), using a fixed 10 µg/ml concentrations of the cutinase/esterase, and varying concentrations (0-30 µg/ml) of an immobilized carboxylesterase.¹⁸

Outcome: Use of the specific dual-enzyme system led to (A) a significant improvement in the ratio of MHET with respect to TPA (i.e., the ratio was reduced), as desired. However, (B) significant levels of MHET were still present. Further, (C) perhaps owing to the reduced MHET-based inhibition, TPA and MHET levels both increased.

Therefore, enzymatic degradation has thus far not succeeded in making the recycling of TPA generated from post-consumer PET back into PET viable, mainly because the TPA that is generated exists in a mixture with other degradation intermediates such as OET, BHET and MHET. So, although enzymatic degradation remains a desirable goal for every one of the reasons listed in the previous section (from the viewpoint of Green Chemistry), and also because it produces no side-products that cannot be resolved into TPA upon further esterase treatment, the goal has not yet been achieved.

PET enzymatic degradation/recycling:

A summary of the philosophy and approach of the new proposal that is presented in this work.

- 1) Making improvements in PET-hydrolyzing cutinases/esterases alone worsens the problem.** Cutinases that hydrolyze PET are required to bind to solid PET. In proportion with their ability to bind to solid PET, therefore, such enzymes happen to become titrated onto the surface of PET. This titration naturally depletes the enzyme population that is available in aqueous solution.²³
- 2) Depletion of enzyme from solution (due to enzyme binding to PET) is the main problem.** We argue that it is this depletion that underlies the fact that mixtures of TPA and other degradation intermediates are always obtained, from every PET hydrolysis reaction, regardless of how efficient an enzyme is (at hydrolyzing PET and its degradation intermediates which have the same polymer backbone chemistry as PET).^{18,25}
- 3) Cutinases/esterases are actually more efficient at degrading the degradation intermediates than they are at degrading PET, but degradation intermediates still accumulate.** It is a fact that is known to all who have worked with these enzymes that cutinases such as TfCut2, and LCC, efficiently generate TPA from both BHET and MHET, but also that the very same enzymes generate large amounts of OET/BHET/MHET that remain unresolved into TPA, as residues in solution, when they act upon PET, without degrading these into TPA (despite being able to do so more efficiently than they are able to degrade PET).^{18,23,25} It is a known fact that PET hydrolysis reactions can have TPA and MHET present in a ratio of 60:40, at the end of a long incubation that lasts a few days.
- 4) Cutinases/esterases are actually capable, but unavailable, to degrade the degradation intermediates into TPA.** Accumulation of OET/BHET/MHET should ideally not have occurred if PET-hydrolyzing cutinases/esterases happen to be both able to degrade MHET more efficiently than PET, and also available to do so, during PET hydrolysis. We point out that these enzymes are indeed able to degrade OET, BHET and MHET (which are all less hydrophobic than PET, and sparingly soluble in water, and which can diffuse into and out of enzyme active sites) more

efficiently than they are able to degrade PET^{26,27} (which is hydrophobic and consists of densely packed chains of polymers that are insoluble). Even so, because these enzymes bind to PET, owing to their surface hydrophobicity, and then remain preoccupied with PET, they do not remain available in solution to degrade the degradation intermediates and the TPA molecules that escape into solution, when an enzyme performs a hydrolysis reaction on the surface of solid PET.^{23,24} We argue, therefore, that the titration of the cutinase/esterase enzyme population onto the surface of PET is the primary reason for the accumulation of residual and unresolved OET/BHET/MHET, since there is no enzyme available in solution to resolve OET, BHET and MHET into TPA. We propose that this situation persists for as long as there is any solid (undegraded) PET still left (and available) to titrate away all hydrolyzing enzyme molecules away from solution. We argue that this situation is only likely to get worse with the further improvement of the abilities of different enzymes to bind to PET and hydrolyze it, if attention is not paid to placing enzymes in solution for the specific purpose of hydrolyzing OET, BHET and MHET into TPA.

- 5) **The solution probably lies in the making available of a second enzyme; one that is specifically deployed in solution.** Thus, we argue that the only way of resolving the OET, BHET and MHET that accumulates in the solution around solid PET is to make a different enzyme available for degrading these molecules, in concert with the action of the cutinase/esterase upon solid PET, i.e., a second enzyme that does not either bind to, or hydrolyze, PET but which is able to degrade OET, BHET and MHET.
- 6) **A two-fold division of labor.** The two enzymes of a dual-enzyme system would ideally engage in a two-fold division of labor; one in terms of the chemicals that the two enzymes work upon, i.e., PET, on the one hand, and PET's degradation intermediates, on the other hand; and the other in terms of the locations at which the two enzymes perform their work, i.e., one on the surface of solid PET, and the other in the solution around solid PET. With such a division of labor, neither enzyme would interfere either physically, or chemically, with the work being performed by the other enzyme.
- 7) **Release of MHET-based inhibition as a bonus, rather than as a goal.** It may be noted that if an enzyme degrades MHET in the solution around PET, the levels of MHET in the vicinity of PET's surface would reduce, thus relaxing the MHET-based inhibition of cutinase/esterases working at PET's surface. Thus, the need to resolve OET, BHET and MHET into TPA, in the solution around PET, in order to improve the quality of TPA, and the need to release the inhibition of PET-hydrolyzing enzymes by MHET, are both served by the same approach, namely to deploy a OET/BHET/MHET hydrolyzing enzyme in the solution around PET, so that the degradation intermediates of PET are further resolved into TPA concomitantly with their generation.
- 8) **Carboxylesterases are probably best suited to playing the role of 'second' enzyme.** Carboxylesterases are already known to degrade MHET.¹⁸ We think that carboxylesterases are ideally suited to degrading small aliphatic as well as aromatic and other esters, because the folds of the polypeptide backbones are somewhat homologous to those of cutinases/esterases, but their active sites tend to be much deeper and less hydrophobic than those of PET-hydrolyzing enzymes, causing carboxylesterases to be incapable of binding to PET (due to PET being unable to access the catalytic residues which are buried away deep with the active site, and also due to PET being too hydrophobic to bind to an active site that is more hydrophilic than the active sites of cutinases/esterases).

PET enzymatic degradation/recycling:

A summary of what we have achieved using the approach outlined above.

As explained above, enzymatic degradation of PET comes with many benefits from the viewpoint of Green Chemistry.

Much prior work in this area has been done. Many excellent enzymes have been discovered, and it may be anticipated that more such enzymes will be discovered, in due course.

The main issue that remains, however, is the incomplete degradation of PET, with the generation of degradation intermediates that remain in reaction mixtures as residues.

Our arguments and proposals are in favor of the possible complete degradation of PET through the use of an additional enzyme.

We demonstrate that the complete degradation of PET can be achieved by using an additional enzyme that fulfills multiple criteria.

- (1) Demonstrated extreme thermostability (demonstrated in this paper),
- (2) Demonstrated extreme solubility (demonstrated in this paper),
- (3) Demonstrated extreme producibility (demonstrated in this paper),
- (4) Demonstrated extreme substrate versatility (demonstrated in this paper),
- (5) Demonstrated inability to bind to PET (demonstrated in this paper),
- (6) Demonstrated inability to perform any significant hydrolysis of PET (demonstrated in this paper),
- (7) Demonstrated ability to work with the cutinase, LCC (demonstrated in this paper), and
- (8) Demonstrated ability to outperform LCC, when working in concert with LCC, yielding the highest yields of TPA ever shown, and also the lowest accumulation of degradation intermediates ever shown.

Our approach, reasoning and results point to a possible way forward, and help to consolidate views that favor the use of dual-enzyme systems that involve a division of both physical (locational) and chemical (catalytic) labor.

The paper also presents calculations of Green Metrics (Energy Economy Factor, Environmental Factor, and Environmental Energy Impact) to support the Green Advances made through this work.

Section 2. Materials and methods

Molecular docking and MD Simulation.

Molecular docking and MD simulation studies were performed to determine residues likely to be involved in OET binding and hydrolysis in TTCE. The structure file for TTCE (RCSB PDB ID: 1UFO) was subjected to the Protein Preparation Wizard²⁸ to obtain a reliable all-atom structure. As the ligand used for docking, the initial structure file for an oligo-ethylene terephthalate (OET) chain of four MHET residues [2HE-(MHET)₄] was prepared using 2D Sketcher. Energy minimization was performed using the Schrödinger LigPrep module. Docking studies were performed using the Schrödinger Glide module,²⁹ with XP-Dock scoring function. The receptor grid was generated to create a 3D space in which the ligand was docked. Using XP-visualizer, docking scores and penalties were determined as detailed in Table S1. The Schrödinger Prime MMGBSA module³⁰ was employed to more accurately calculate the binding affinity of 2HE-(MHET)₄ to TTCE. The Schrödinger Desmond package was employed to perform MD simulations, using docked structures as the initial structures for the simulation. Desmond's System Builder tool was employed to prepare the system, and the OPLS3e force-field was applied, with simulation carried out in an orthorhombic box filled with TIP3P water as solvent. The system was neutralized through addition of counter ions and salt ions (concentration maintained at 150 mM NaCl). The Desmond MD simulation tool was used to carry out 75 ns of simulation, using a recording interval of 10 ps, within NPT ensemble at 300 K, using the Nose–Hoover chain thermostat,³¹ and 1.0013 bars, using an integration time-step of 2 fs, and the Martyna–Tobias–Klein barostat.³² A default cut-off radius of 9.0 Å was specified for Coulombic interactions. MD simulation trajectories were analyzed using Desmond's simulation interaction diagram (SID) tool. The free energy of binding (ΔG_{bind}) was calculated using the OPLS3e force-field and VSGB 2.1 solvation model, through application of the following equation: $\Delta G_{\text{bind}} = E_{\text{Complex}} - E_{\text{Ligand}} - E_{\text{Receptor}}$, in which E is the energy associated with the van der waals, hydrophobic and electrostatic interactions in the ligand-protein complex (E_{Complex}), during ligand desolvation (E_{Ligand}) and during receptor desolvation (E_{Receptor}), respectively.

Gene cloning, expression, purification and identity-confirmation of TTCE, LCC and LCC-TTCE fusion.

The gene encoding TTCE was cloned from the genomic DNA of *Thermus thermophilus* into a pET23a plasmid, between Nde I and Hind III restriction sites, using the following primers to introduce restriction sites for cloning: NdeI-TTCE Forward : 5' TATATACATATGAGGGTTCGGACCGAGCGGCTC 3'. TTCE-HindIII : 5' ATATATAAGCTTCCGTGCCTCAAGCCAGTG 3'. The pET23a plasmid containing the TTCE gene was transformed into the BL21pLysS* expression host, induced to express TTCE with a C-terminal 6xHis affinity tag, using 1 mM IPTG (Isopropyl β -d-1-thiogalactopyranoside) at a culture optical density of 0.6, and induction for 5.5 hours at 37 °C following which cells were harvested through centrifugation, and the pellet obtained dissolved in bacterial cell lysis buffer (50 mM sodium dihydrogen phosphate, 150 mM NaCl and 10 mM imidazole) and subjected to sonication in the presence of lysozyme, before further centrifugation at 12,000 rpm to settle cell debris. The lysate was loaded onto a pre-equilibrated Ni-NTA (Nickel-nitrilotriacetic acid) column, for IMAC affinity chromatographic purification, using a wash with 35 mM imidazole, protein elution with 250 mM imidazole, and collection of protein in seven 1 ml fractions, followed by SDS-PAGE analysis. The gene encoding LCC (Genbank: AEV21261) was codon optimized for expression in *Escherichia coli*, gotten synthesized by a commercial service-provider (Biotech Desk Pvt. Ltd., Hyderabad, India), cloned without the gene segment encoding the signal peptide (between the Bam HI and Hind III restriction

sites of the pQE30 vector) to produce a construct possessing an N-terminal 6xHis polyhistidine tag, and then expressed and purified using IMAC affinity chromatography from XL1Blue cells, using standard protocols. The gene encoding the LCC-TTCE fusion, incorporating a 22 residues-long polypeptide segment (GGGSGGSGGSG)₂ as linker between the LCC and TTCE segments, was created in two steps (through PCR reactions) and cloned between the Nde I and Not I restriction sites of pET23a, to produce (and purify, using IMAC affinity chromatography) a C-terminally 6xHis-tagged LCC-TTCE fusion, using the BL21pLysS* strain of *E. coli*. The gel band corresponding to a protein of the expected size was excised, subjected to trypsin treatment using the ProteoProfile™ Trypsin In-Gel Digest Kit (Sigma Aldrich, Product Code PP 0100), mixed with the MALDI matrix, α -Cyano-4-hydroxycinnamic acid (Sigma Aldrich, Product Code C8982) in a ratio of 1:1, and subjected to MALDI-Q-TOF analyses on a Synapt G2S-HDMS mass spectrometer (Waters), in single-stage (MS) mode, followed by matching of masses of observed peptides with the masses of peptides generated through *in silico* trypsin digestion of TTCE (using ProtParam and the ExPASy server).

Spectroscopic and chromatographic characterization of the folded state of TTCE.

(1) Quaternary structure. Size exclusion chromatography (SEC), glutaraldehyde crosslinking, and dynamic light scattering (DLS) were used to examine the oligomeric status of TTCE. *Firstly*, following IMAC chromatography, eluted samples were concentrated to a volume of 500 μ l and loaded onto a Superdex-75 Increase 10/300 GL gel filtration column (GE-healthcare), pre-equilibrated with 25 mM sodium dihydrogen phosphate buffer of pH 8.0, on an AKTA workstation, to compare the elution volume of TTCE with a calibration standard, using SEC. *Secondly*, to check for the presence of higher order oligomers of TTCE, protein purified through SEC was incubated with 0.05%, 0.1% and 0.2% (v/v) of glutaraldehyde, for 10 minutes at room temperature, with stopping of the reaction through boiling of samples in dye-containing, 5x SDS-PAGE loading buffer, at 99 °C, for 5 minutes, followed by electrophoretic analyses of samples on a 13% acrylamide SDS-PAGE, with analyses of gels based on the known preservation of glutaraldehyde crosslinks during SDS-treatment and boiling, and observations of gel band mobilities. *Thirdly*, dynamic light scattering (DLS) based characterization was done in phosphate-buffered saline at pH 8.0 on a Wyatt QELS+ Heleos 8 instrument.

(2) Tertiary structure. The tertiary structure of TTCE was examined through assessment of its folded state based on fluorescence spectroscopic examination of the wavelength of maximal fluorescence emission of its intrinsic fluorescence, derived from its single tryptophan residue. The occurrence of a wavelength of maximal emission that was significantly lower than ~353 nm was used as evidence of the shielding of the tryptophan residue from the aqueous solvent through the formation of a tertiary structure.

(3) Secondary structure. The secondary structure of TTCE was examined on a Chirascan™ circular dichroism spectrometer (Applied Photophysics Ltd.), using a quartz cuvette of 1 mm path length, TTCE at a concentration of 0.2 mg/ml in 25 mM phosphate buffer of pH 8.0, and mean residue ellipticity (MRE) calculated at each wavelength, to create the CD spectrum, using the formula: $MRE = (\theta \times \text{mean residue weight} \times 100) / (1000 \times \text{concentration in mg/ml} \times \text{pathlength in cm})$, where θ was the raw ellipticity measured in millidegrees.

Spectroscopic and chromatographic characterization of the equilibrium thermal stability of TTCE's folded state.

Firstly, thermal stability was assessed using circular dichroism (CD) through the thermal denaturation of TTCE (by heating between 20 °C to 90 °C, at a rate of 1°C/min) with concomitant collection of CD spectra on a Chirascan™ (Applied photophysics) spectrometer fitted with a Peltier block, using a protein concentration of 0.2 mg/ml in 25 mM phosphate buffer, pH 8.0, in a 2 mm path length (quartz) cuvette.

Secondly, thermal stability was assessed using differential scanning calorimetry (DSC) through the thermal denaturation of TTCE (heating between 20 °C and 90 °C, at a rate of 90 °C/h, and cooling between 90 °C and 20 °C, at a rate of 60 °C/h) with concomitant measurement of enthalpic changes on a differential scanning calorimeter (MicroCal VP-DSC), using a protein concentration of 0.5 mg/ml, following 5 cycles of heating and cooling of the control (phosphate) buffer, to generate the baseline, and data concerning heat required to unfold the protein being extracted from the system and measured, over the temperature range in which a difference in the rate of change of temperature between sample and control (reference) cells could be observed. A specific heat capacity *versus* temperature graph was obtained, and the area under the baseline-subtracted, concentration-normalized graphs was then estimated to measure the change in enthalpy associated with protein unfolding, with the peak of the transition curve assessed to be the measured melting temperature.

Thirdly, thermal stability was assessed using fluorescence spectroscopy through the thermal denaturation of TTCE (heating between 20 °C and 90 °C) with concomitant measurement of changes in the tertiary structure of TTCE through monitoring of red shifts in TTCE's fluorescence emission maximum wavelength, on a steady-state fluorimeter (FluoroMax, HORIBA), during thermal unfolding, with sample excitation performed at 295 nm, and emission recorded between 300 and 400 nm.

Spectroscopic characterization of the chemical stability of TTCE's folded state.

(1) *Equilibrium measurements.* Chemical stability was assessed using CD and fluorescence spectroscopy, for samples of TTCE incubated overnight with the chemical denaturants, urea, and guanidium hydrochloride (Gdm.HCl), using the monitoring of changes in spectral characteristics (i.e., CD spectral MRE values at 222 nm, to monitor changes in TTCE's secondary structure; and fluorescence emission spectral maximum wavelengths, to monitor changes in TTCE's tertiary structure) as a function of the unfolding of 0.2 mg/ml TTCE, in the range of 0-8 M urea, or 0-6 M Gdm.HCl. Values of C_m (i.e., the denaturant concentration at which half the molecules in any population have undergone unfolding) were determined for unfolding by the two denaturants.

(2) *Kinetic measurements.* To study the kinetics of unfolding, TTCE was incubated with Gdm.HCl (different concentrations in the range of 5-7 M) for two hours, with monitoring of changes in secondary structure as a function of time, and with calculation of the fraction un-folded with respect to time of incubation (2 hours) thereafter being plotted and fitted, using the 'expDecay1' function of the software, Origin Pro 2018. The respective rates of unfolding (K_u) determined from the plots were utilized to obtain the half-chevron plot (natural logarithm of K_u *versus* activity of denaturant [D] determined from the concentration of denaturant [Gdm.HCl]). The slope of the half- chevron plot was used to calculate the rate of unfolding in absence of denaturant ($K_{u,w}$). This rate indicates the kinetic stability (i.e., resistance to unfolding) at a particular temperature. The relevant equations used were (1) $K_u = K_{u,w} \cdot e^{m_u \cdot D}$, in which $K_{u,w}$ is the rate of unfolding in absence of denaturant; and (2) $D = 7.5[\text{Gdm.HCl}] / (7.5 + [\text{Gdm.HCl}])$, in which D is the activity of denaturant and m_u is the slope of half chevron plot.³³

Activity of LCC and TTCE upon different esters.

(1) *Absorption measurements using turbidogenic or chromogenic substrates.* To assess TTCE's ability to act upon short and long chain aliphatic esters, the enzyme was reacted with 1-Naphthyl butyrate (2.5

mM), and 4-Nitrophenylpalmitate (250 μ M), at temperatures ranging from 50 $^{\circ}$ C to 100 $^{\circ}$ C, releasing naphthol and para-nitrophenol, which were quantified using absorbance measurements at 235 nm, and 410 nm, respectively. The catalytic potential of LCC in comparison with TTCE (2 μ M each) was compared using the following two substrates: (i) 4-Nitrophenylpalmitate (250 μ M) at 70 $^{\circ}$ C for 5 hours, and (ii) Fluorescein dilaurate (250 μ M) at 60 $^{\circ}$ C for 6 hours.

(2) *Measurements using RP-HPLC-based separation of DIs and TPA.* Further, TTCE's potential to hydrolyze the following substrates was assessed and compared with LCC's potential: (i) PET films and granules, and (ii) PET's degradation intermediates (DIs), specifically bis-hydroxyethyl-terephthalate, or BHET (incubation for 12 hours, at 60 $^{\circ}$ C). For the work with PET granules, granules were either used directly with enzyme (incubation for 50 h, at 60 $^{\circ}$ C), or dissolved in hexafluoroisopropanol (HiMedia Laboratories) and then dried in an incubator-shaker at 50 $^{\circ}$ C to form a film which was washed with distilled water and phosphate buffer of pH 8.0, prior to reaction with enzyme (incubation for 4 days, at 60 $^{\circ}$ C). Activity was also assessed using commercially-sourced PET films (Goodfellow, Product code: GF25214475) of thickness 0.25 mm, which were cut into circular discs of radius 3 mm, washed with 1% SDS at 50 $^{\circ}$ C for 30 minutes, and then with de-ionized water and ethanol, using the same temperatures and time periods, before overnight air-drying of the ethanol and use in enzymatic degradation experiments (incubations for 50 h, at 60 $^{\circ}$ C). The products of degradation, namely, TPA, BHET and MHET, were quantified using a Shimadzu HPLC equipped with a photodiode array (PDA) detector and a LiChrospher[®] RP-18 column (5 μ m particle size, L \times I.D. 25 cm \times 4.6 mm), with dilution of samples in a 1: 1 ratio with acetonitrile, prior to injection of 20 μ l of this dilution into the column, for separation using a mobile phase of phosphate buffer of pH 2.5 (Solvent A) and methanol (Solvent B), run conditions consisting of 3 timed stages (0-5 minutes, 25% B; 5-22 minutes, 25%-100 % B; 22-27 minutes, 25% B), and measurement of the absorbance of DIs at 240 nm, with quantification of products through reckoning of the area under each elution.

(3) *Scanning Electron Microscopy.* PET polymers in the form of circular films of ~6 mm diameter were examined using SEM after the enzymatic treatment. The untreated and enzyme-treated films were washed with 1% SDS, water and ethanol. Films were air dried and sputter-coated with gold of 5 nm thickness. Coated films were mounted on aluminum stubs using carbon tape, and SEM imaging was done using a Jeol Field emission Scanning Electron Microscope, with a beam accelerating voltage of 15 keV.

Section 3. Supporting Tables

Table S1: Docking scores from Glide-XP-dock and binding scores from Prime-MMGBSA calculations, using Schrödinger software.

Hydrolase	Ligand	Dock Score	Glide emodel	Prime Energy	MMGBSA ΔG binding
LCC	2HE-(MHET) ₄	-5.06	-74.71	-10336.95	-71.95
TTCE	2HE-(MHET) ₄	-4.87	-80.7	-9423.35	-72.93

Table S2: Comparison of thermal (CD and intrinsic fluorescence), kinetic (Gdm.HCL induced unfolding measured using CD) and thermodynamic stabilities (DSC) of TTCE and LCC

	Apparent T_m from CD	Red shift from intrinsic fluorescence	Rate of kinetic unfolding in water ($K_{u,w}$)	Enthalpy of unfolding using DSC (Kcal/moles)
TTCE	No unfolding observed till 90 °C	No change observed till 90 °C	$2.6 \times 10^{-20} \text{ s}^{-1}$	$\Delta H = 1915.87$
LCC	83.7 °C	80 °C	N.D.	Two state transition $\Delta H_1, \Delta H_2$: 302.1, 231.9

Section 4. Supporting Figures

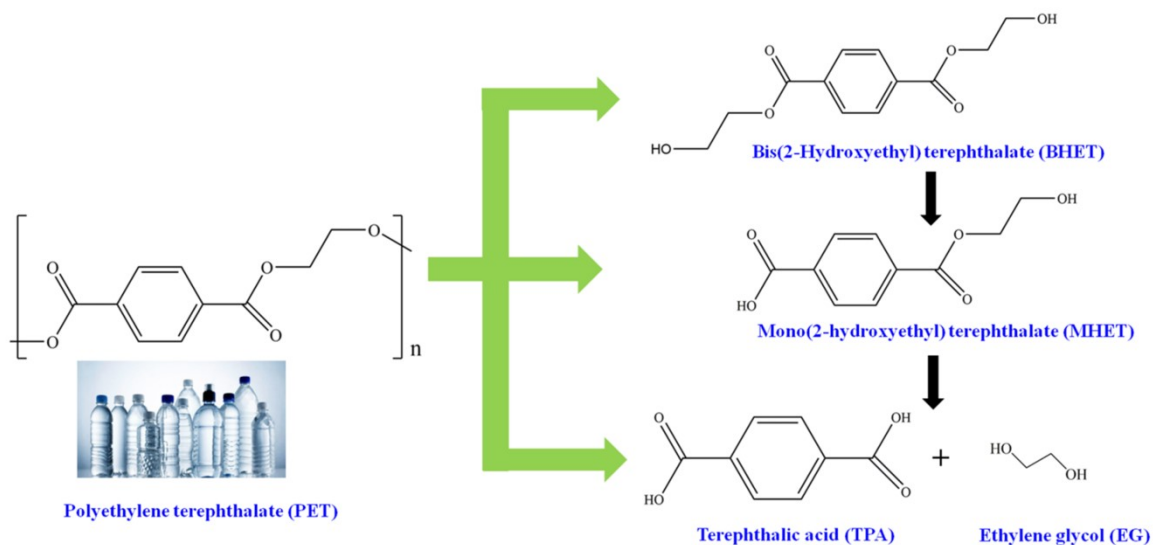


Figure S1: Enzymatic breakdown of polyethylene terephthalate (PET) or oligoethylene terephthalate (OET) into different degradation intermediates (DIs). In PET, the 'n' is large, whereas in OET (not shown) the 'n' is small. The 'exolytic' action of enzymes upon PET/OET can generate the terminal degradation product, terephthalic acid (TPA), along with ethylene glycol (EG). Exolytic action can also generate degradation intermediates such as Bis-(2-hydroxyethyl) terephthalate (BHET), and Mono-(2-hydroxyethyl) terephthalate (MHET). Multiple 'endolytic' actions of enzymes upon PET generate OETs.

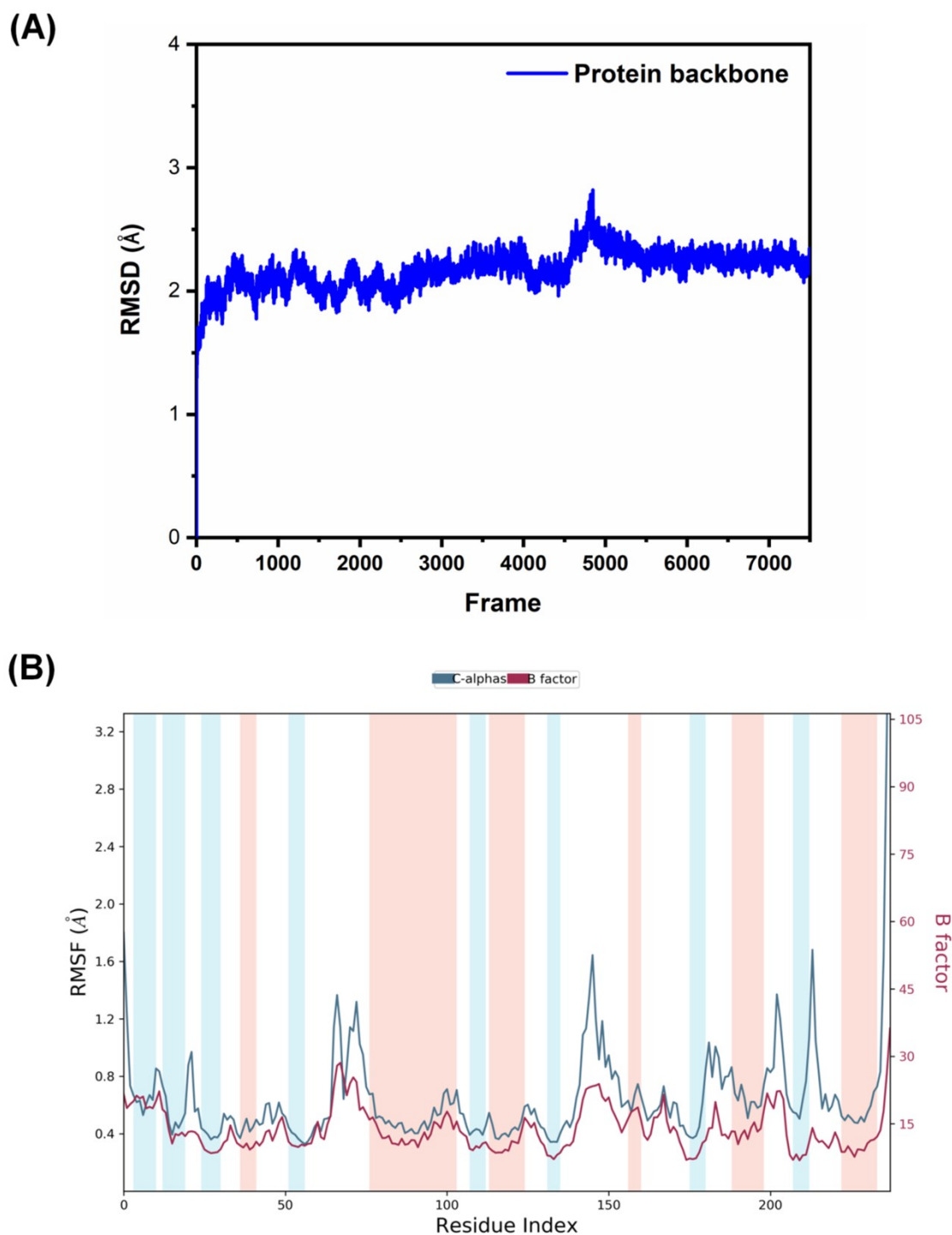


Figure S2: Molecular dynamics simulation of TTCE-2HE-(MHET)₄ for 75 ns shows (A) dynamically stable trajectory as indicated by the flattened root mean-square deviation (RMSD) in the protein structure relative to the initial structure. (B) rootmean-square fluctuations (RMSF) indicating the extent of flexibility at each residue position. The peaks denote the position of flexible residues in TTCE most likely to interact with short chain PET.

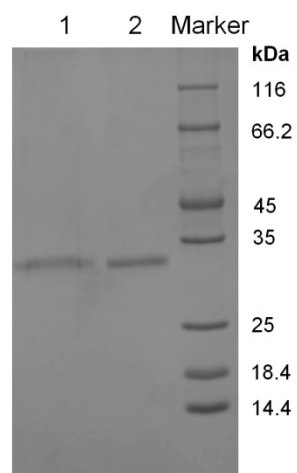


Figure S3: SDS-PAGE binding assay for PET film treated with 2 μ M LCC for a duration of 8 hours. Lane 1: LCC bound to PET film, Lane 2: LCC in solution.

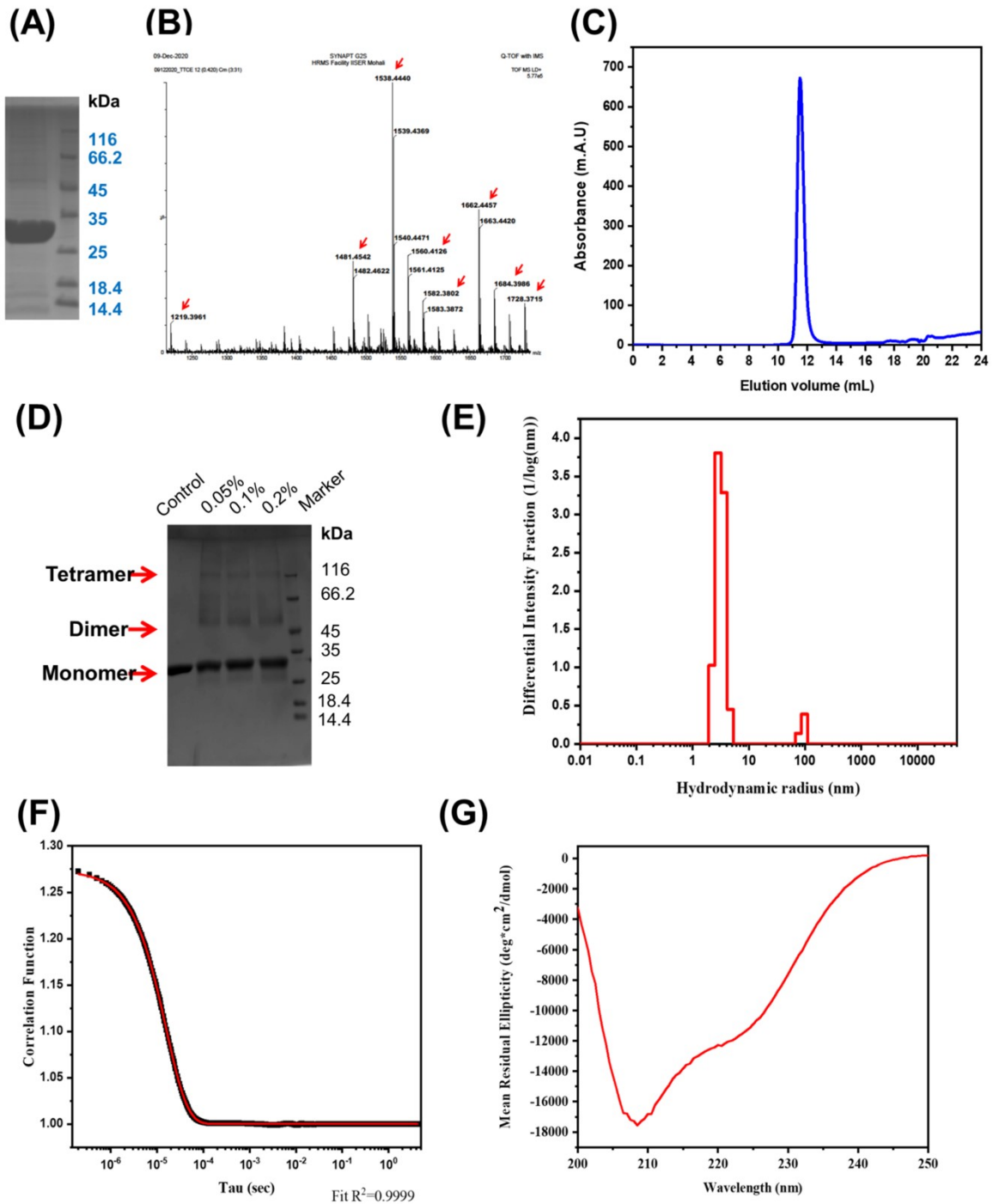


Figure S4: (A) SDS-PAGE lanes showing the eluted fraction obtained during purification of TTCE. (B) MALDI-Q-TOF peptide mass fingerprint of TTCE, with red arrows representing peptide masses observed that matched with masses of in silico trypsin-digested TTCE. (C) Size exclusion chromatogram of TTCE, monitoring elution of protein absorbing at 280 nm (characteristic absorption of tryptophan residues). (D) Outcome of cross-linking of TTCE by varying concentrations of glutaraldehyde. (E) Dynamic light scattering results, showing distribution of sizes of TTCE. (F) Correlation function for the light scattering results. (G) Circular Dichroism spectrum of the mixed α/β structure of TTCE.

The recombinant ~26 kDa protein is TTCE. Purified TTCE was electrophoresed on SDS-PAGE, and the band displaying mobility corresponding to a mass of ~26 kDa was excised and subjected to mass spectrometric analysis, as shown in Figure S4A. The masses of peptide peaks obtained experimentally were matched with the masses of peptide peaks generated through *in silico* tryptic digestion of TTCE. In Figure S4B, peaks marked with red arrows identify the many masses that matched the expected (*in silico* digestion-generated) masses, to an accuracy of 1 Da, thus confirming TTCE's identity.

TTCE is predominantly dimeric. We assessed the quaternary structural status of TTCE through a combination of size exclusion chromatography (SEC), glutaraldehyde crosslinking, and dynamic light scattering (DLS) experiments. The chromatogram in Figure S4C shows that TTCE elutes at 11.51 ml from a Superdex-75 Increase column, which places its native molecular weight between ~26 kDa and ~52 kDa, i.e., between the elution volumes expected for a monomer and a dimer, towards the dimer. That TTCE exists as an equilibrium population of monomers and dimers was also established through crosslinking by glutaraldehyde (a homo-bi-functional chemical reagent that covalently crosslinks proteins placed in close proximity, through reaction of the reagent's aldehyde group with protein N-termini or the ϵ -amino groups of lysine residues), as shown in Figure S4D. Notably, TTCE's crystal structure provides scope for dimerization through the formation of anti-parallel beta sheets between monomers. The hydrodynamic radius obtained by DLS experiments also supports an equilibrium of monomers and dimers. Weight-fractions of population, plotted in Figure S4E (with the correlation function shown in Figure S4F), suggest a radius of 3.10 nm (or a diameter of ~6.2 nm) for 93.51% of the TTCE population, a value which is larger than the radius of a monomer (~2.4 nm, as reckoned from the crystal structure), and smaller than that of a dimer. Notably, the DLS experiments also showed that a small fraction of the population exists as oligomers or aggregates.

TTCE contains a mix of alpha and beta structures. The circular dichroism (CD) spectrum of TTCE is shown in Figure S4G. It is dominated by α -helices; with low negative intensity at ~218 nm, owing to the presence of β -sheet content, and high negative intensity at ~208 nm, owing to helical content and the presence of random coils, which is in agreement with the determined structure of the enzyme.

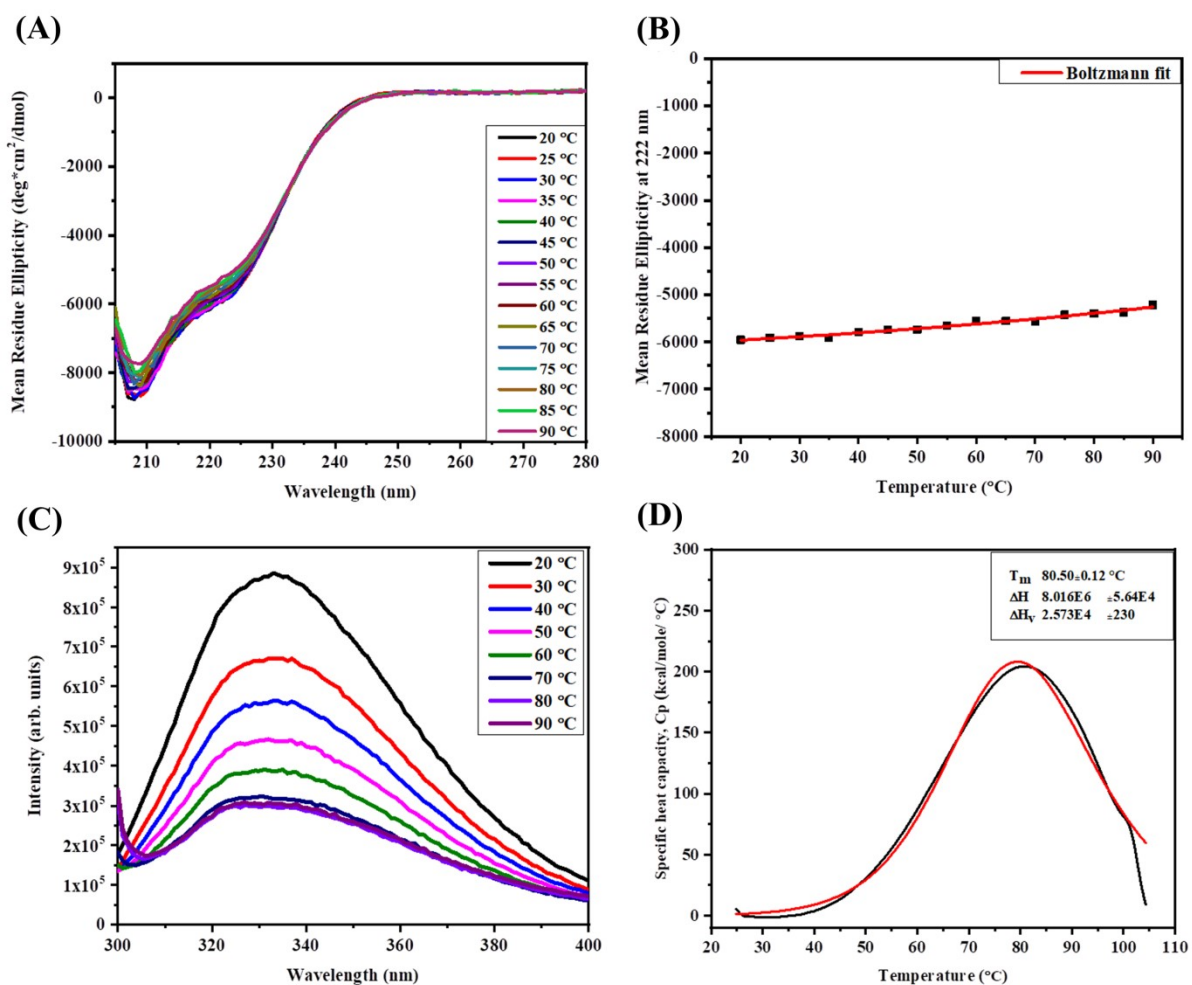


Figure S5: Thermal and thermodynamic stabilities of TTCE. (A) Changes in secondary structure of TTCE (CD spectra) as a function of heating to different temperatures between 20 °C and 90 °C, (B) the Boltzmann fit of the MRE values at 222 nm at this temperature range. (C) Changes in fluorescence (intensity and wavelength shift) owing to change in microenvironment of tryptophan in TTCE upon heating from 20 °C to 90 °C. (D) Enthalpic changes associated with heating of TTCE (Differential Scanning Calorimetry profile, showing the data in black, and the fitting in red).

TTCE is extraordinarily thermally stable. We assessed the thermal stability of TTCE through a combination of circular dichroism (CD), fluorescence spectroscopic and differential scanning calorimetric (DSC) studies. Figure S5A shows that there are no variations in the far-UV CD spectrum of purified TTCE as a function of increasing temperature, during heating of the enzyme between 20 °C and 90 °C. The Boltzmann fit of the MRE values at 222 nm plotted against the corresponding temperature indicated that more than 90% of the secondary structure remains intact at 90 °C (Figure S5B). The monitoring of intrinsic fluorescence derived from TTCE's single tryptophan, which is expected to display a solvent-dependent, red-shifting of the fluorescence emission maximum value, from its native value of ~333 nm (for the folded, and native, protein) to longer wavelengths, owing to protein unfolding, shows that there is no such red shifting observed, as shown in Figure S5C. This establishes that there are no significant tertiary structural changes accompanying the heating of TTCE, over the same temperature range (from 20 °C to 90 °C). Notably, a gradual drop in fluorescence intensity with temperature is observed, due to the increased probability of thermal de-excitation of the excited tryptophan moiety. The overall conclusion from the above data is that there is effectively no unfolding of the secondary or tertiary structures of TTCE, even at very high temperatures. This

conclusion was further tested through micro-calorimetric (DSC) studies. As shown in Figure S5D, the T_m from the up-scan (i.e. heating of TTCE from 20 °C to 90 °C) was estimated to be 80.5 °C, with a significant change in enthalpy (8.016×10^6 Joules/mole) seemingly associated with this structure-melting or unfolding transition, which is suggestive of significant thermodynamic stability in TTCE's native three-dimensional structure. Notably, the enthalpic transition in DSC is seen at 80.5 °C, although changes in secondary and/or tertiary structure are not noted to occur even up to a temperature of 90 °C, as already mentioned. This suggests that TTCE could exist in a molten globular state at temperatures between 80.5 °C and 90 °C, with the enthalpic transition not being paralleled by any significant change in structure. At any rate, these studies show that TTCE can work at temperatures exceeding the glass-transition temperatures of almost all forms of semi-crystalline and crystalline post-consumer PET.

TTCE appears to be extraordinarily chemically stable, in equilibrium measurements. We next assessed the chemical stability of TTCE through CD and fluorescence studies to explore the energetics of the enzyme's unfolding at 25 °C, during overnight incubation, by denaturants such as urea, and guanidium hydrochloride (Gdm.HCl). CD data plotting changes in mean residue ellipticity (MRE) as a function of denaturant concentration are shown in Figure S6A-S6D. With urea, Figure S6A and Figure S6B, respectively, show CD spectra and variations in the intensity of the CD signal at 222 nm, and TTCE is seen to retain the same MRE value at 222 nm over denaturant concentrations ranging from 0.0-8.0 M urea. This demonstrates that even overnight incubation in 8 M urea has no effect upon TTCE's structure. Figure S6C and Figure S6D show CD spectra and variations in the intensity of the CD signal at 222 nm with varying concentrations of Gdm.HCl. TTCE is seen to retain the same MRE values at 222 nm over denaturant concentrations ranging from 0.0-4.5 M Gdm.HCl, demonstrating that even overnight incubation in 4.5 M Gdm.HCl has no effect upon TTCE's structure. However, it is observed that 6 M Gdm.HCl completely destroys TTCE's secondary structure, through a cooperative melting transition with a C_m of around 5.1 M Gdm.HCl, as can be seen in Figure S6C. Notably, these results are in keeping with the known facts that (a) urea disrupts mainly hydrogen bonds, while Gdm.HCl disrupts hydrogen bonds as well as electrostatic interactions, and that (b) proteins commonly display a C_m with urea that is about twice the C_m obtained with Gdm.HCl.³⁴ The high C_m of 5.1 with Gdm.HCl indicates that the C_m with urea would be 10.2 M (exceeding the solubility of urea). The data thus indicates that hydrogen bonds determine TTCE's stability to a lower degree than electrostatic interactions, and also that urea is unable to unfold the protein by attempting to disrupt hydrogen bonds alone. Further, we also examined spectra for intrinsic fluorescence emission owing to tryptophan residues. These are shown as Figure S6E and Figure S6F, respectively, for urea and Gdm.HCl. From these panels, it is evident that the tertiary structure of TTCE is largely intact up to a urea concentration of nearly 8 M, and a Gdm.HCl concentration of nearly 4.5 M, indicating that it is not merely TTCE's secondary structure which is highly stable, but also its tertiary structure. Notably, the unfolding of TTCE by concentrations of Gdm.HCl exceeding 4.5 M is observed to be accompanied by a dramatic increase in the protein's fluorescence quantum yield, together with a red shift in the protein's wavelength of maximal emission, as can be seen in Figure S6F. The increase in quantum yield appears to owe to a change in the environment of tryptophan, which appears to have been released from quenching. The appearance of an emission band at 307 nm appears to owe to cessation of energy transfer between a nearby tyrosine residue (separated by 8 Å from the tryptophan residue), and tryptophan, in the native structure, allowing visibility of the tyrosine's fluorescence (no longer subject to energy transfer) upon TTCE's unfolding.

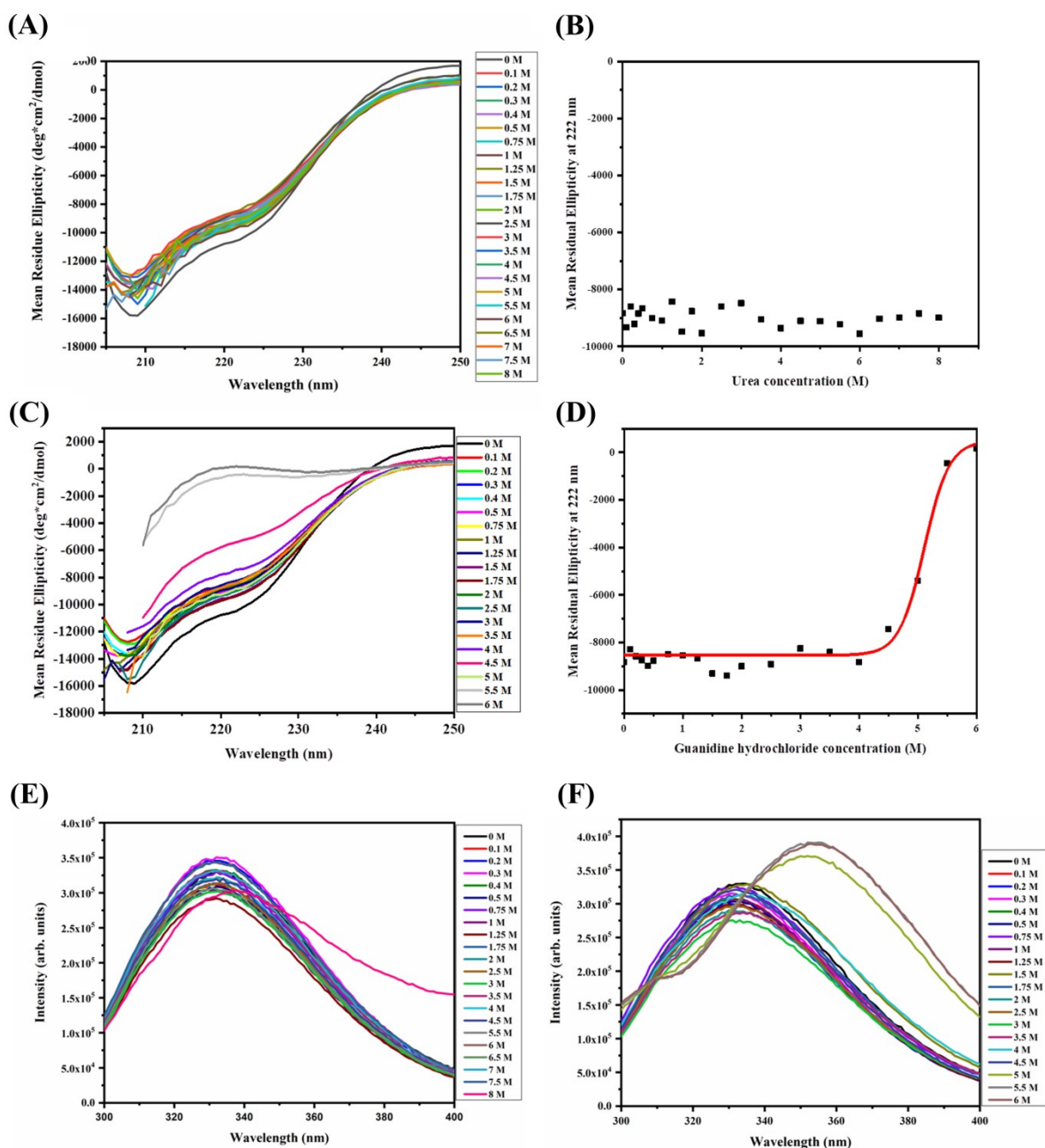


Figure S6: Chemical (equilibrium) stabilities of TTCE: (A) CD spectra of TTCE incubated overnight with varying concentrations of (0 M to 8 M) of urea and, (B) the Boltzmann fit showing changes in MRE at 222 nm at these concentration ranges of urea. (C) CD spectra of TTCE incubated overnight with varying concentrations of (0 M to 6 M) of Gdm.HCl. and, (D) the Boltzmann fit showing changes in MRE at 222 nm at these concentration ranges of Gdm.HCl. **Fluorescence spectra** of TTCE incubated overnight with varying concentrations of (E) (0 M to 8 M) of urea and (F) (0 M to 6 M) of Gdm.HCl.

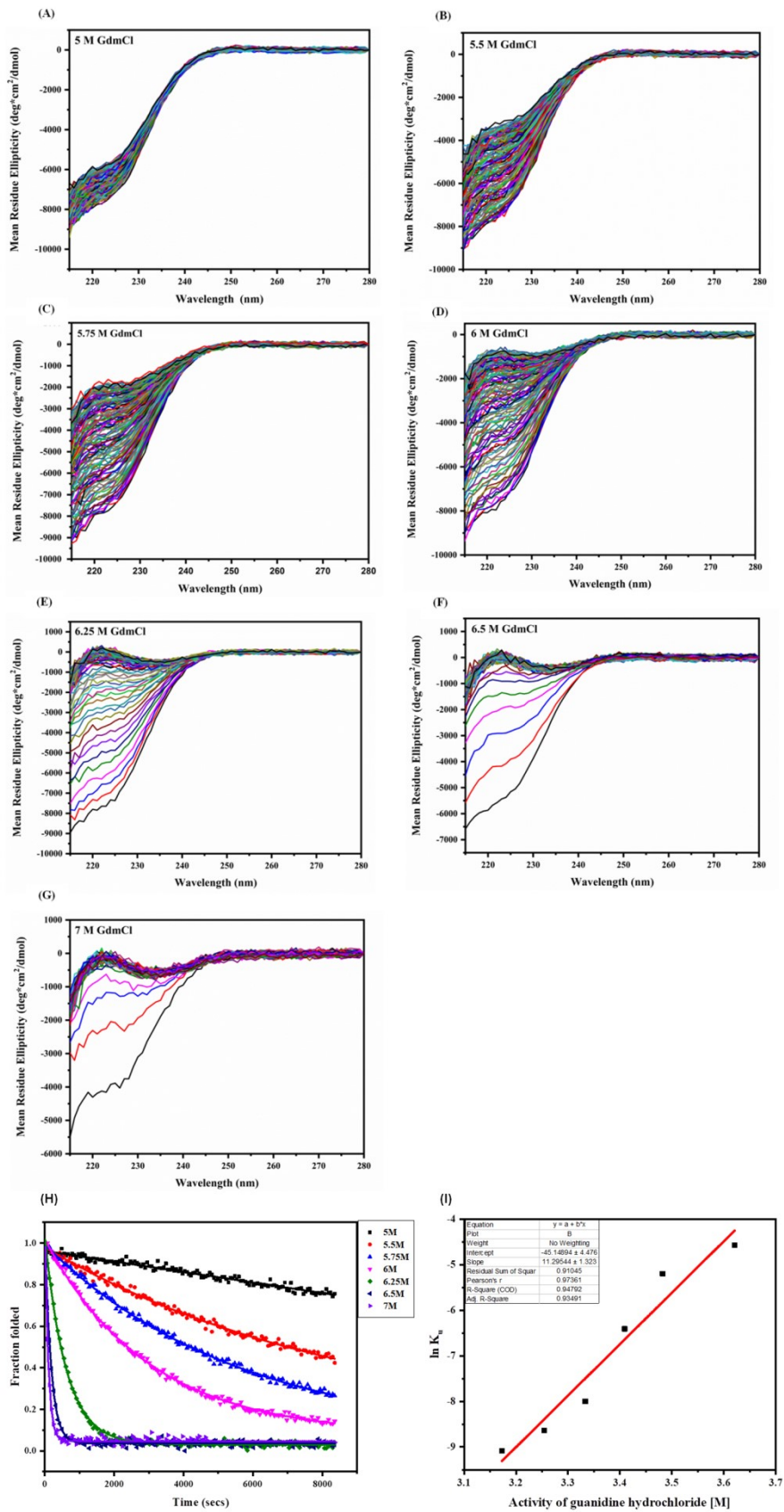


Figure S7: Chemical (Kinetic) stability of TTCE in the presence of (A to G) 5 M to 7 M Gdm.HCl (also known as Gdm.Cl). (H) Fraction folded versus time plot at Gdm.HCl concentrations in the range of 5 M to 7 M, during the course of 2 hours of incubation with the denaturant. (I) Half-chevron plot obtained from the rates of unfolding determined for different Gdm.HCl concentrations.

TTCE also appears to be extraordinarily chemically-stable, in kinetic measurements. To determine the energetic features of TTCE, kinetic studies based on Gdm.HCl unfolding were performed using CD spectroscopy. MRE values at 222 nm, plotted as a function of time (at a particular denaturant concentration, over a period of 2 hours), were used to derive rates of unfolding at each Gdm.HCl concentration, based on the spectra shown in Figures S7A-to-S7G, covering Gdm.HCl concentrations ranging from 5.0-7.0 M. Subsequently, rates of unfolding of TTCE in the absence of denaturant were calculated from the plot of fraction folded *versus* time, shown in Figure S7H. The slope of the half-Chevron plot (m_u), presented in Figure S7I, was 11.29. The rate of unfolding of TTCE in water ($K_{u,w}$), calculated from equation (1), was $2.6 \times 10^{-20} \text{ s}^{-1}$. For comparison, it may be mentioned that many proteins from the hyperthermophilic archaeon, *Pyrococcus furiosus*, have rate constants for unfolding in water (without denaturant) of the order 10^{-15} s^{-1} .^{35,36} The rate of unfolding obtained for TTCE was thus about 5 orders of magnitude slower than that of the proteins from *P. furiosus*, i.e., $2.6 \times 10^{-20} \text{ s}^{-1}$. This slow rate is indicative of the extraordinarily high kinetic stability of TTCE to chemical denaturation.

TTCE acts upon small aliphatic esters and BHET. Figure S7A shows TTCE's action upon 1-Naphthyl butyrate (7.4 μM enzyme; 2 mM substrate), with an optimum temperature of $\sim 50^\circ\text{C}$, with the enzyme retaining 85 % of its maximal activity at 80°C , owing to its high thermal stability (demonstrated in the previous section). Figure S7B shows TTCE's action upon an aliphatic long-chain ester, para-nitrophenyl palmitate (1 μM enzyme; 500 μM substrate), with a similar optimum temperature of $\sim 50^\circ\text{C}$, with 72 % of its maximal activity retained even at 100°C . These experiments demonstrate that, upon production in *Escherichia coli*, the amino acid sequence of TTCE folds into a three-dimensional structure that is not merely thermally-stable, but also optimally active at high temperatures as well as active over a wide range of temperatures (including extremely high temperatures), as would be expected for any enzyme designed by nature to fold within *Thermus thermophilus*; of course, only as long as the enzyme were itself able to fold to the designated native structure in a different environment (such as the cytoplasm of *E. coli*) through, e.g., co-translational folding of its polypeptide chain. Many carboxylesterases are known to additionally hydrolyse complex aromatic substrates, and not just small aliphatic substrates.

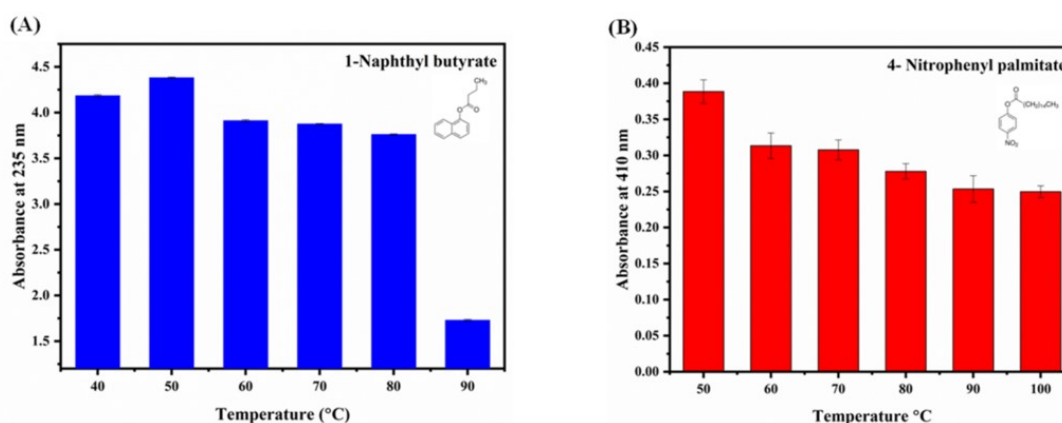


Figure S8: Activity of TTCE upon different substrates. (A) 1-Naphthyl butyrate, quantified through measurement of absorbance at 235 nm. (B) 4-Nitrophenyl palmitate, quantified through measurement of absorbance at 410 nm.

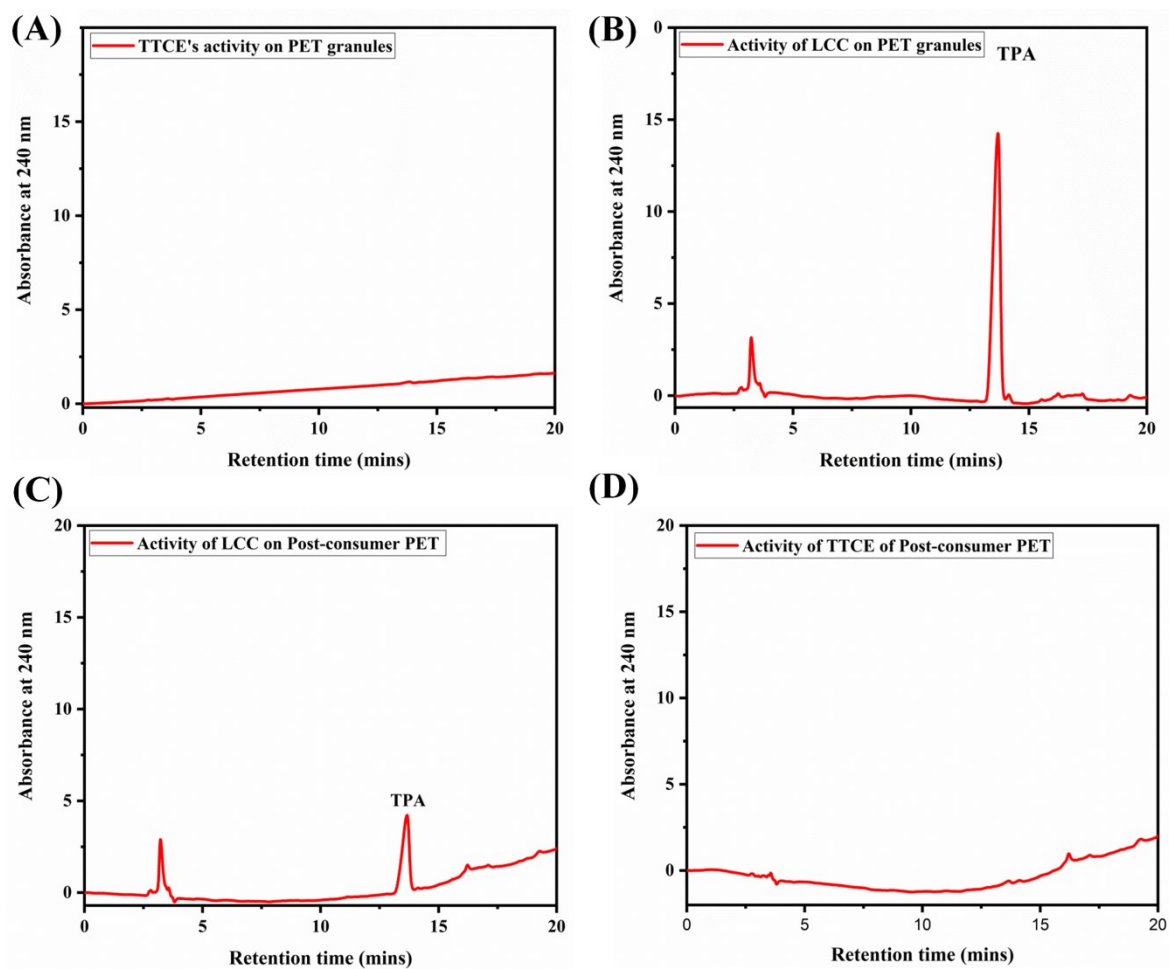


Figure S9: HPLC chromatogram showing enzymatic activity of (A) TTCE on intact PET granules; (B) LCC on intact PET granules; (C) LCC on post-consumer; (D) TTCE on post-consumer.

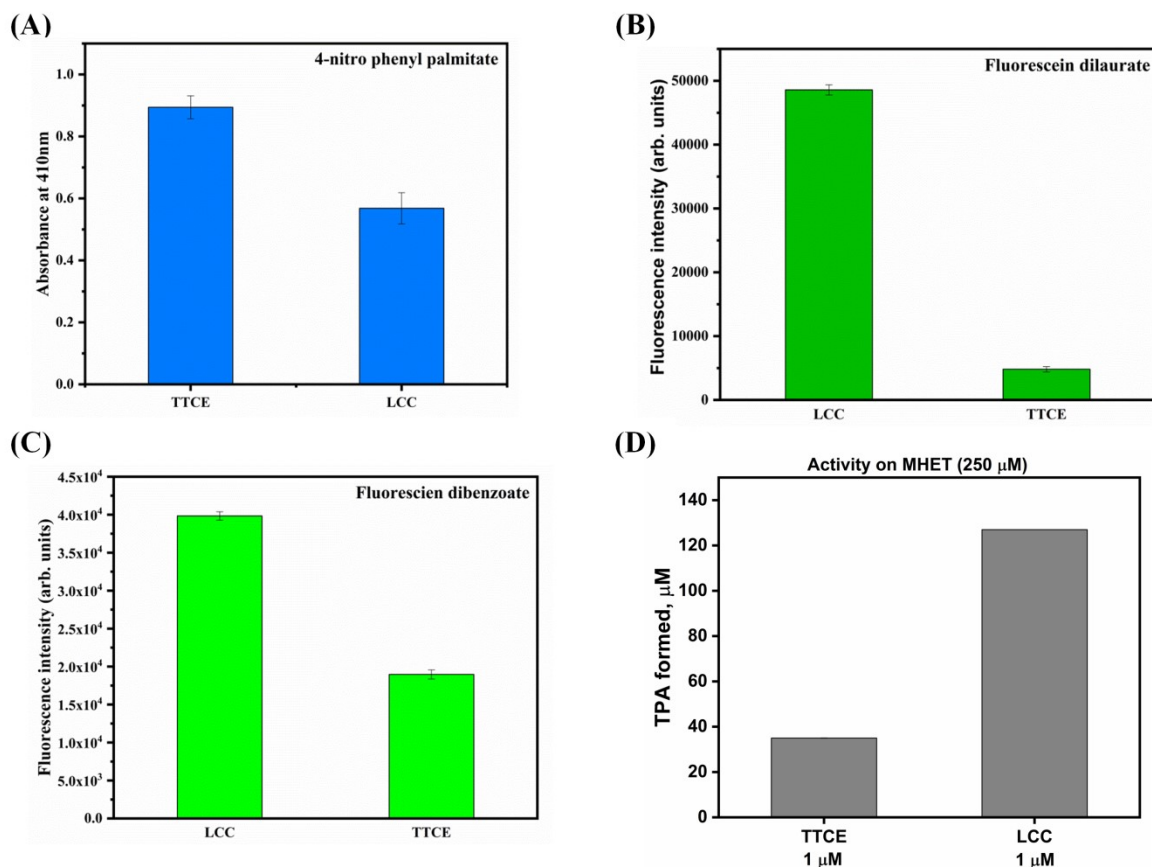


Figure S10: Comparison of the activities of TTCE and LCC upon (A) para-nitrophenyl palmitate. (B) Fluorescein dilaurate. (C) Fluorescein di benzoate. (D) MHET.

- We compared the activities of LCC and TTCE with an aliphatic long-chain ester, para-nitrophenyl palmitate, using identical reaction conditions (2 μM enzyme; 500 μM substrate; 70 °C; 5 hours). TTCE is about twice as efficient as LCC at hydrolysing palmitate ester.
- When similar experiments to the one above were performed with fluorescein dilaurate, the activity of TTCE was found to be 10-fold lower than that of LCC,
- In contrast to both of the above experiments, which used different substrates of relatively small size, when fluorescein dibenzoate, a third substrate, was used in place of fluorescein dilaurate, TTCE was found to perform only ~2-fold poorer than LCC, and not ten times poorer (as with fluorescein dilaurate).
- LCC demonstrates more than 3 folds activity on MHET as compared to TTCE.

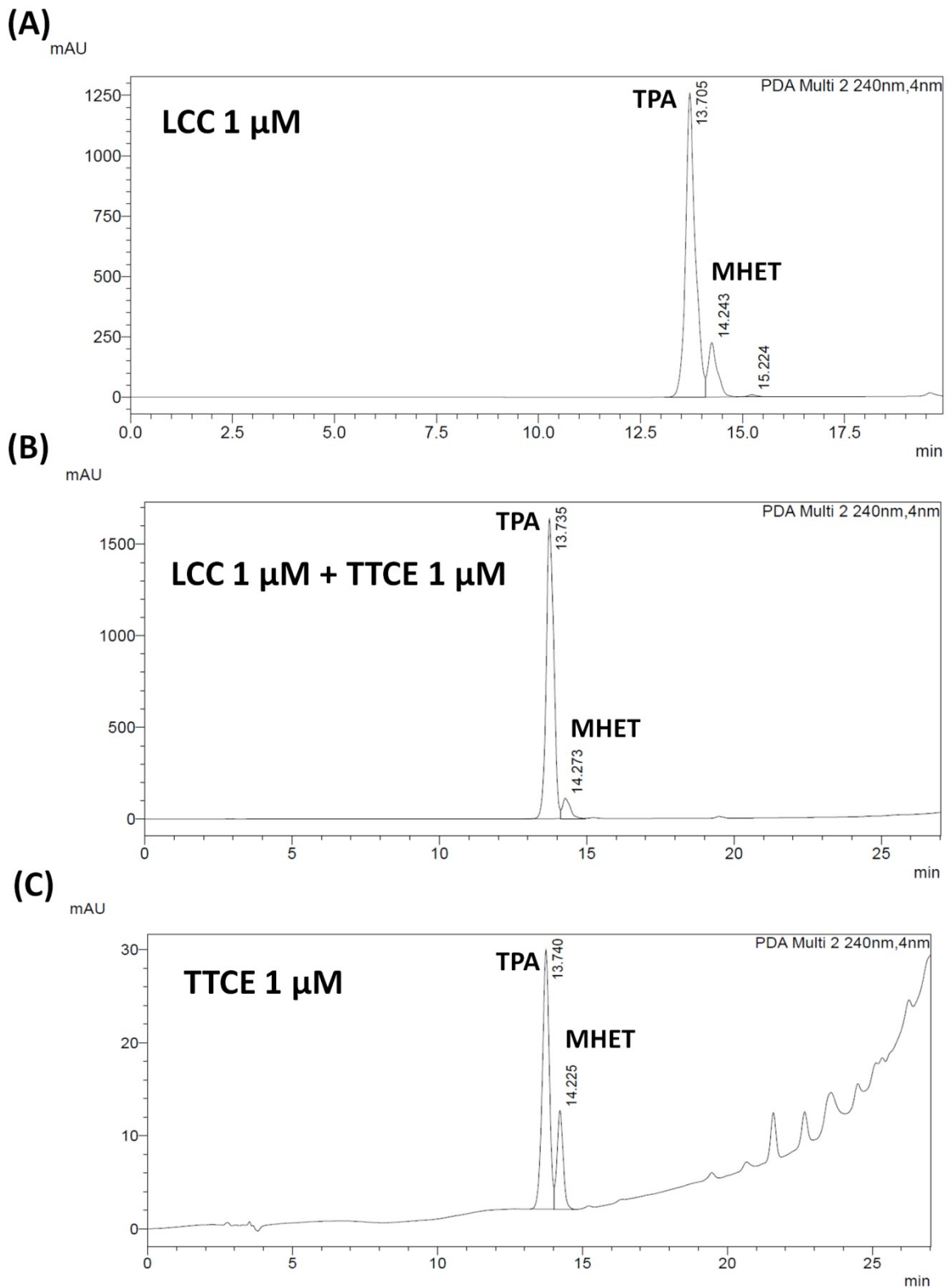


Figure S11: HPLC chromatogram suggesting synergistic action of LCC and TTCE shown by (A) 1 μ M LCC, (B) 1 μ M each of TTCE and LCC, (C) 1 μ M TTCE alone.

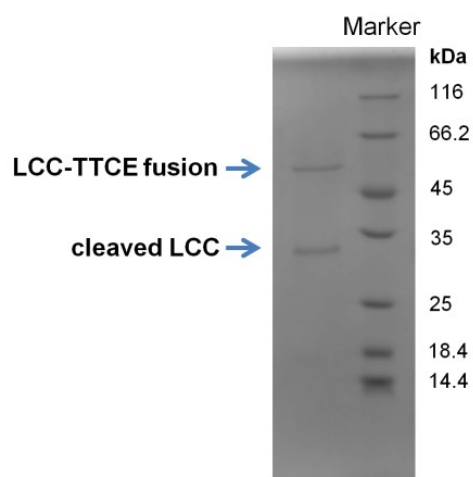
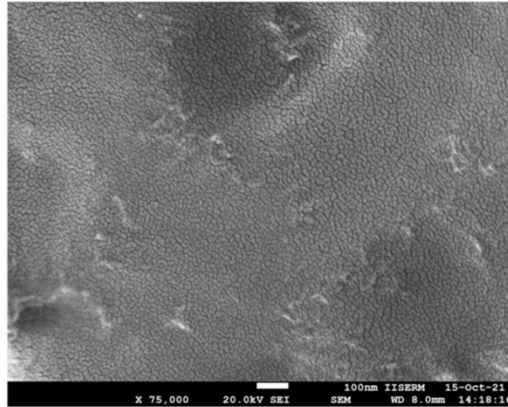
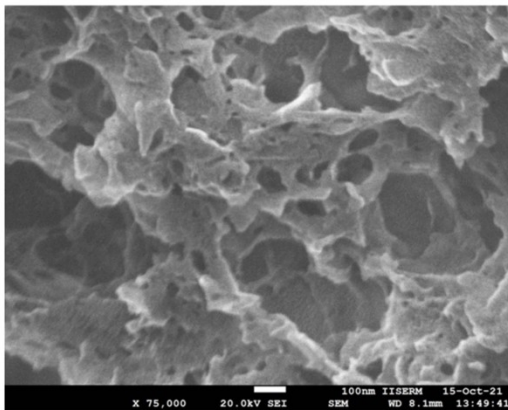


Figure S12: SDS-PAGE binding assay for PET film treated with 2 μ M LCC-TTCE fusion, for a period of 50 hours. The fraction shows the two populations corresponding to the intact LCC-TTCE fusion construct bound to PET, and the LCC bound to PET after the proteolytic degradation of the linker between the LCC and TTCE, suggesting the release of some molecules of TTCE in the solution.

(A)



(B)



(C)

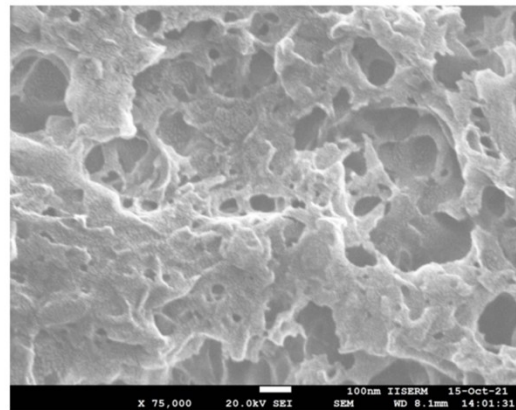


Figure S13: Scanning electron microscopy (SEM) images of the surfaces of PET films subjected to exposure to the LCC-TTCE fusion construct, and the LCC+TTCE enzyme cocktail. Magnified images are presented. (A) Untreated PET surface (75000X). (B) Surface treated with the TTCE+LCC enzyme cocktail (75000X). (C) Surface treated with the LCC-TTCE enzyme fusion (75000X). Greater invasion of the PET surface appears to be achieved with the LCC+TTCE enzyme cocktail and the LCC-TTCE enzyme fusion than with LCC alone.

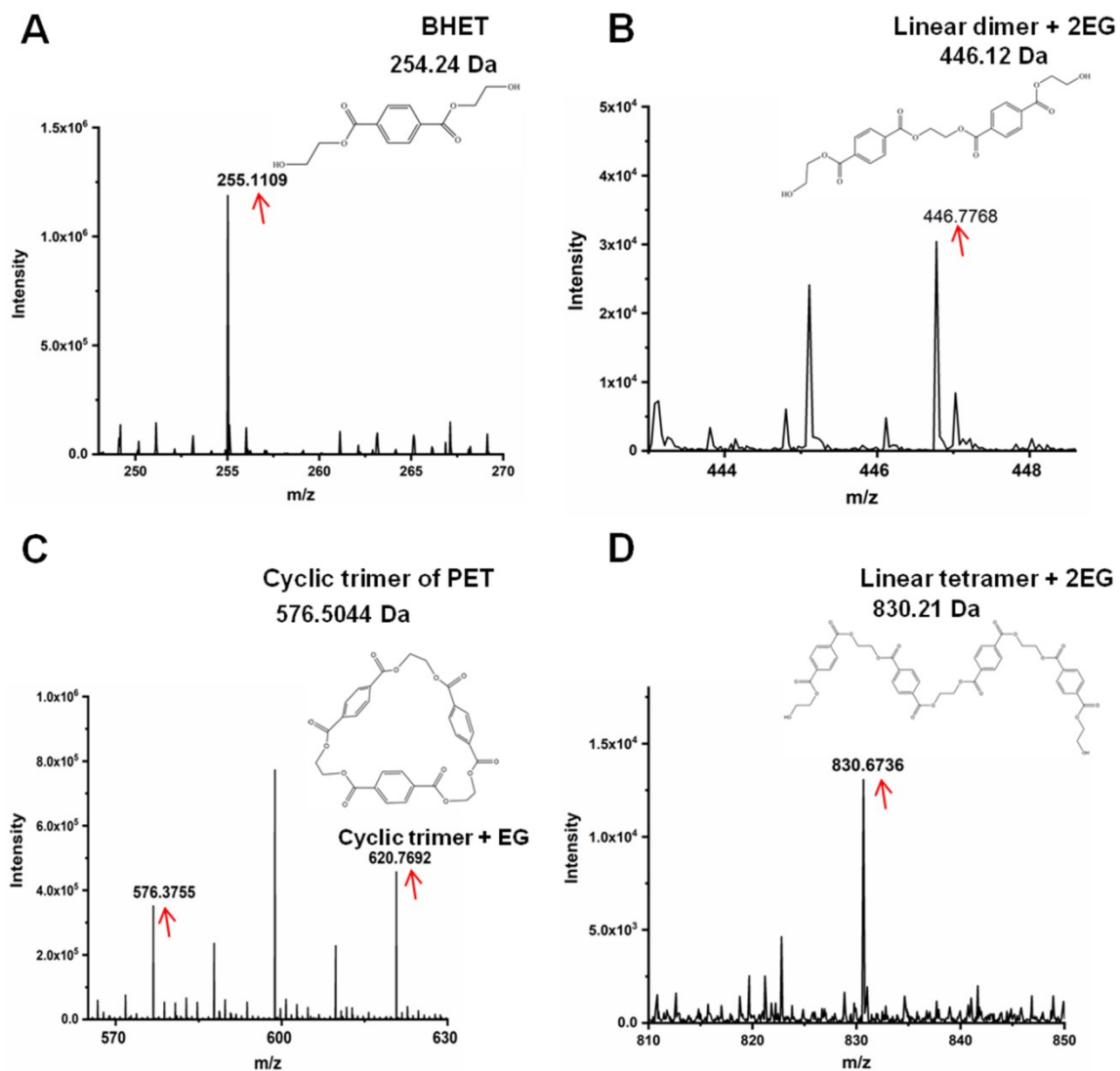


Figure S14: LC-coupled ESI Q-TOF MS based characterization of additional degradation products in solution: (A) BHET, and OETs including (B) Linear dimer flanked by 2 ethylene glycol groups, (C) Cyclic trimer (D) Linear tetramer flanked by 2 ethylene glycol groups.

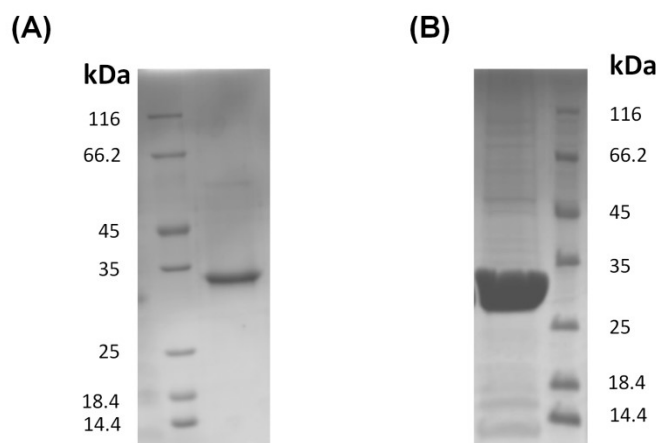


Figure S15: (A) LCC, (B) TTCE protein yields obtained from *E.coli* (1 litre culture).

4. References

1. F. Lionetto, C.E. Corcione, A. Rizzo, A. Maffezzoli, Production and Characterization of Polyethylene Terephthalate Nanoparticles. *Polymers*, 2021, **13**, 3745.
2. Damayanti, H.-S. Wu, Strategic Possibility Routes of Recycled PET. *Polymers*, 2021, **13**, 1475.
3. D. Danso, J. Chow, W.R. Streit, Plastics: environmental and biotechnological perspectives on microbial degradation. *Applied and Environmental Microbiology*, 2019, **85**:e01095-19.
4. B. C. Knott, E. Erickson, M. D. Allen, J. E. Gado, R. Graham, F. L. Kearns, I. Pardo, E. Topuzlu, J. J. Anderson, H. P. Austin, G. Dominick, C. W. Johnson, N. A. Rorrer, C. J. Szostkiewicz, V. Copié, C. M. Payne, H. L. Woodcock, B. S. Donohoe, G. T. Beckham & J. E. McGeehan, Characterization and engineering of a two-enzyme system for plastics depolymerization. *Proceedings of the National Academy of Sciences of the United States of America*, 2020, **117**(41), 25476-25485.
5. R. Wei and W. Zimmermann, Microbial enzymes for the recycling of recalcitrant petroleum-based plastics: how far are we? *Microbial Biotechnology*, 2017 **10**(6):1308-1322.
6. F. Kawai, T. Kawabata and M. Oda, Current knowledge on enzymatic PET degradation and its possible application to waste stream management and other fields. *Applied Microbiology and Biotechnology*, 2019, **103**(11), 4253–4268.
7. E. Erickson, T.J. Shakespeare, F. Bratti, B.L. Buss, R. Graham, M.A. Hawkins, G. König, W.E. Michener, J. Miscall, K.J. Ramirez, N.A. Rorrer, M. Zahn, A.R. Pickford, J.E. McGeehan and G.T. Beckham, Comparative Performance of PETase as a Function of Reaction Conditions, Substrate Properties, and Product Accumulation. *ChemSusChem*, 2021, **14**, 1–12.
8. P. Turner, G. Mamo, and E.N. Karlsson, Potential and utilization of thermophiles and thermostable enzymes in biorefining. *Microbial cell factory*, 2007, **6**, 9.
9. S. F. Loibl, Z. Harpaz, R. Zitterbart and O. Seitz, Total chemical synthesis of proteins without HPLC purification. *Chemical Science*, 2016, **7**, 6753.
10. V. Tournier, C. M. Topham, A. Gilles, B. David, C. Folgoas, E. Kamionka, M. Desrousseaux, H. Texier, S. Gavalda, M. Cot, E. Guémard, M. Dalibey, J. Nomme, G. Cioci, S. Barbe, M. Chateau, I. André, S. Duquesne & A. Marty, An engineered PET depolymerase to break down and recycle plastic bottles. *Nature*, 2020, **580**, 216.

11. C. Vieille and G. J. Zeikus, Hyperthermophilic enzymes: sources, uses, and molecular mechanisms for thermostability. *Microbiology and molecular biology reviews : MMBR*, 2001, **65(1)**, 1-43.
12. B. Geyer, G. Lorenz and A. Kandelbauer, Recycling of poly(ethylene terephthalate) – A review focusing on chemical methods. *Express Polymer Letters*, 2016, **10(7)**, 559–586.
13. G.P. Karmakar. Regeneration and Recovery of Plastics. Reference Module in *Materials Science and Materials Engineering*. 2020, B978-0-12-820352-1.00045-6.
14. J. C. Sadler and S. Wallace, Microbial synthesis of vanillin from waste poly(ethylene terephthalate). *Green Chemistry*, 2021, **23**, 4665–4672.
15. H.T. Kim, J.K. Kim, H.G. Cha, M.J. Kang, H.S. Lee, T.U. Khang, E.J. Yun, D.H. Lee, B.K. Song, S.J. Park, J.C. Joo and K.H. Kim, Biological Valorization of Poly(ethylene terephthalate) Monomers for Upcycling Waste PET. *ACS Sustainable Chemistry and Engineering*, 2019, **7(24)**, 19396–19406.
16. J. Slapnik, G. Kraft, T. Wilhelm and A. Lobnik, Purification of recycled terephthalic acid and synthesis of polyethylene terephthalate. *International Circular Packaging Conference*, 2019.
17. A.H. Tullo, Plastic has a problem; is chemical recycling the solution? *Chemical and engineering news*, 2019, **97(39)**. (<https://cen.acs.org/environment/recycling/Plastic-problem-chemical-recycling-solution/97/i39>)
18. M. Barth, A. Honak, T. Oeser, R. Wei, M. R. Belisário-Ferrari, J. Then, J. Schmidt and W. Zimmermann, A dual enzyme system composed of a polyester hydrolase and a carboxylesterase enhances the biocatalytic degradation of polyethylene terephthalate films. *Biotechnology Journal*, 2016, **11(8)**, 1082–1087.
19. R. Wei, T. Oeser, J. Schmidt, R. Meier, M. Barth, J. Then and W. Zimmermann, Engineered bacterial polyester hydrolases efficiently degrade polyethylene terephthalate due to relieved product inhibition. *Biotechnology and Bioengineering*, 2016, **113(8)**, 1658–1665.
20. J. Then, R. Wei, T. Oeser, A. Gerds, J. Schmidt, M. Barth, & W. Zimmermann, A disulfide bridge in the calcium binding site of a polyester hydrolase increases its thermal stability and activity against polyethylene terephthalate. *FEBS Open Bio*, 2016, **6(5)**, 425–432.
21. J. Then, R. Wei, T. Oeser, M. Barth, M. R. Belisário-Ferrari, J. Schmidt, & W. Zimmermann, Ca²⁺ and Mg²⁺ binding site engineering increases the degradation of polyethylene terephthalate films by polyester hydrolases from *Thermobifida fusca*. *Biotechnology Journal*, 2015, **10(4)**, 592–598.
22. C. Silva, S. Da, N. Silva, T. Matamá, R. Araújo, M. Martins, S. Chen, J. Chen, J. Wu, M. Casal, & A. Cavaco-Paulo, Engineered *Thermobifida fusca* cutinase with increased activity on polyester substrates. *Biotechnology Journal*, 2011, **6(10)**, 1230–1239.
23. D. Ribitsch, A.O. Yebra, S. Zitzenbacher, J. Wu, S. Nowitsch, G. Steinkellner, K. Greimel, A. Doliska, G. Oberdorfer, C.C. Gruber, K. Gruber, H. Schwab, K. Stana-Kleinschek, E.H. Acero and G.M. Guebitz, Fusion of binding domains to *Thermobifida cellulolytica* cutinase to tune sorption characteristics and enhancing PET hydrolysis. *Biomacromolecules*, 2013, **14(6)**, 1769–1776.
24. D. Ribitsch, E.H. Acero, A. Przylucka, S. Zitzenbacher, A. Marold, C. Gamerith, R. Tscheließnig, A. Jungbauer, H. Rennhofer, H. Lichtenegger, H. Amenitsch, K. Bonazza, C.P. Kubicek, I. S. Druzhinina, G.M. Guebitz, Enhanced cutinase-catalyzed hydrolysis of polyethylene terephthalate by covalent fusion to hydrophobins. *Applied and Environmental Microbiology*, 2015, **81**, 3586–3592.
25. F. Yan, and R. Wei, Q. Cui, U.T. Bornscheuer, and Y.J. Liu, Thermophilic whole-cell degradation of polyethylene terephthalate using engineered *Clostridium thermocellum*. *Microbial Biotechnology*, 2021, **14(2)**, 374–385.
26. J.A. Bååth, K. Borch, K. Jensen, J. Brask and P. Westh, Comparative Biochemistry of Four Polyester (PET) Hydrolases. *ChemBioChem*, 2021, **22(9)**, 1627–1637.
27. R.P. Magalhães, J.M. Cunha, and S.F. Sousa, Perspectives on the role of enzymatic biocatalysis for the degradation of plastic pet. *International Journal of Molecular Sciences*, 2021, **22(20)**, 11257.

28. G. Madhavi Sastry, M. Adzhigirey, T. Day, R. Annabhimoju and W. Sherman, Protein and ligand preparation: Parameters, protocols, and influence on virtual screening enrichments. *Journal of Computer-Aided Molecular Design*, 2013, **27(3)**, 221–234.
29. R. A. Friesner, R. B. Murphy, M. P. Repasky, L. L. Frye, J. R. Greenwood, T. A. Halgren, P. C. Sanschagrin and D. T. Mainz, Extra precision glide: Docking and scoring incorporating a model of hydrophobic enclosure for protein-ligand complexes. *Journal of Medicinal Chemistry*, 2006, **49(21)**, 6177–6196.
30. M. P. Jacobson, D. L. Pincus, C. S. Rapp, T. J. F. Day, B. Honig, D. E. Shaw and R. A. Friesner, A Hierarchical Approach to All-Atom Protein Loop Prediction. *Proteins: Structure, Function and Genetics*, 2004, **55(2)**, 351–367.
31. G. J. Martyna, M. L. Klein & M. Tuckerman, Nosé – Hoover chains : The canonical ensemble via continuous dynamics Nose-Hoover chains : The canonical ensemble via continuous dynamics. *The Journal of Chemical Physics*, 2007, **97**, 2635.
32. G. J. Martyna, D. J. Tobias, & M. L. Klein, Constant pressure molecular dynamics algorithms. *The Journal of Chemical Physics*, 1994, **101(5)**, 4177–4189.
33. M. J. Parker, J. Spencer & A. R. Clarke, An integrated kinetic analysis of intermediates and transition states in protein folding reactions. *Journal of Molecular Biology*, 1995, **253(5)**, 771–786.
34. J. S. Smith and J. M. Scholtz, Guanidine hydrochloride unfolding of peptide helices: separation of denaturant and salt effects. *Biochemistry*, 1996, **35(22)**, 7292-7.
35. K. A. Luke, C. L. Higgins and P. Wittung-Stafshede, Thermodynamic stability and folding of proteins from hyperthermophilic organisms. *FEBS Journal*, 2007, **274(16)**, 4023–4033.
36. K. Ogasahara, The unusually slow unfolding rate causes the high stability of pyrrolidone carboxyl peptidase from a hyperthermophile, *Pyrococcus furiosus*: Equilibrium and kinetic studies of guanidine hydrochloride- induced unfolding and refolding. *Biochemistry*, 1998, **37(50)**, 17537–17544.